



1 **The Effect of the 2013-2016 High Temperature Anomaly in the Subarctic Northeast Pacific**

2 **(The “Blob”) on Net Community Production**

3 Bo Yang¹, Steven R. Emerson¹, M. Angelica Peña²

4 ¹ School of Oceanography, University of Washington, Seattle, WA 98195, USA

5 ² Institute of Ocean Sciences, Fisheries and Oceans Canada, PO Box 6000, Sidney, BC, Canada,

6 V8L 4B2

7 Corresponding author: Bo Yang (byang9@uw.edu)

8 Email address: Steven R. Emerson (emerson@uw.edu), M. Angelica Peña ([9 \[mpo.gc.ca\]\(mailto:mpo.gc.ca\)\)](mailto:Angelica.Pena@dfp-</p></div><div data-bbox=)

10 Key words: The warm blob, net community production, ocean station Papa

11



12 Abstract

13 A large anomalously warm water patch (the “Blob”) appeared in the NE Pacific Ocean in
14 the winter of 2013–14 and persisted through 2016 causing strong positive upper ocean
15 temperature anomalies at Ocean Station Papa (OSP, 50°N, 145°W). The effect of the
16 temperature anomalies on annual net community production (ANCP) was determined by upper
17 ocean chemical mass balances of O₂ and DIC using data from a profiling float and a surface
18 mooring. Year-round oxygen mass balance in the upper ocean (0 to 91–111 m) indicates that
19 ANCP decreased after the first year when warmer water invaded this area and then returned to
20 the “pre-blob” value (2.4, 0.8, 2.1, and 1.6 mol C m⁻² yr⁻¹ from 2012 to 2016, with a mean value
21 of 1.7 ± 0.7 mol C m⁻² yr⁻¹). ANCP determined from DIC mass balance has a mean value that is
22 similar within the errors as that from the O₂ mass balance but without significant trend (2.0, 2.1,
23 2.6, and 3.0 mol C m⁻² yr⁻¹ with a mean value of 2.4 ± 0.6 mol C m⁻² yr⁻¹). This is likely due to
24 differences in the air-sea gas exchange, which is a major term for both mass balances. Oxygen
25 has a residence time with respect to gas exchange of about one month while the CO₂ gas
26 exchange response time is more like a year. Therefore the biologically induced oxygen saturation
27 anomaly responds fast enough to record annual changes whereas that for CO₂ does not.
28 Phytoplankton pigment analysis from the upper ocean show lower chlorophyll-*a* concentrations
29 and greater relative abundance of picoplankton in the year after the warm water patch entered the
30 area than in previous and subsequent years. Our analysis of multiple physical and biological
31 processes that may have caused the ANCP decrease after warm water entered the area suggests
32 that it was most likely due to changes in plankton community composition.



33 **1 Introduction**

34 Net community production (NCP) in the upper ocean is defined as net organic carbon
35 production, which equals biological production minus respiration. At steady state when
36 integrated over a period of at least one year, the annual NCP (ANCP) is equivalent to the flux of
37 biologically-produced organic matter from the upper ocean to the interior. Both biological
38 production and respiration processes are temperature dependent, and heterotrophic activities such
39 as community respiration and zooplankton grazing are usually considered to be more sensitive to
40 temperature change than autotrophic production (Allen et al., 2005; Brown et al., 2004; Gillooly
41 et al., 2001; López-Urrutia et al., 2006; Regaudie-De-Gioux and Duarte, 2012; Rose and Caron,
42 2007). This implies that rising temperature should lead to enhanced heterotrophy and lower NCP
43 (López-Urrutia et al., 2006). In contrast, it has also been suggested (e.g., Chen and Laws, 2017)
44 that the main effect of temperature on community metabolism is likely due to differences in
45 phytoplankton community composition (e.g. cyanobacteria dominate in warm, oligotrophic
46 waters, whereas diatoms dominate in cold, nutrient-rich areas) rather than to lower temperature
47 sensitivity of phytoplankton production.

48 From the winter of 2013, a large anomalously warm water patch (the “Blob”) appeared
49 in the NE Pacific Ocean (Bond et al., 2015). The “Blob” had stretched from Alaska to Baja
50 California by the end of 2015 (Di Lorenzo and Mantua, 2016) and caused widespread changes in
51 the marine ecosystem, such as geographical shifts of plankton species, harmful algal blooms, and
52 strandings of fishes, marine mammals, and seabirds (Cavole et al., 2016). Here we calculate the
53 ANCP with upper ocean oxygen (O_2) and dissolved inorganic carbon (DIC) mass balances using
54 data from Ocean Station Papa in the NE Pacific (OSP, 50°N, 145°W, Figure 1), to determine if
55 there were significant NCP changes during the anomalous warm event. The monthly Sea Surface



56 Temperature Anomaly (SSTA) at OSP from 2012 to 2016 (Figure 2) indicates that for most of
57 the 1st year (starting from June 2012) sea surface temperature (SST) was lower than usual, but
58 then transitioned to strong positive temperature anomaly from 2013 to 2014. The positive
59 anomaly continued with a magnitude of ~ 2°C to June 2015, and then dropped back to “normal”
60 in the summer of 2016.

61 Our field location is in the subarctic northeast Pacific Ocean at OSP, where repeat
62 hydrographic cruises have been carried out since 1981 by Fisheries and Oceans Canada with a
63 frequency of two to three times per year (Freeland, 2007). A NOAA surface mooring has been
64 deployed at OSP since 2007, for physical and biogeochemical measurements such as
65 temperature, salinity, wind, ocean current, radiation, oxygen and total gas pressure, pH, and
66 carbon dioxide (CO₂) (Emerson et al. 2011; Cronin et al. 2015; Fassbender et al. 2016). In
67 addition, Argo profiling floats have been deployed near OSP since the 2000s (Freeland and
68 Cummins, 2005). The first floats measured only temperature, salinity, and pressure but then
69 measurements of oxygen and nitrate were added (Bushinsky and Emerson, 2015; Johnson et al.,
70 2009). NCP at OSP has been determined using various approaches over the years, including
71 bottle incubations (Wong, 1995), ²³⁴Th methods (Charette et al., 1999), carbon/nutrient
72 drawdown (Fassbender et al., 2016; Plant et al., 2016; Takahashi et al., 1993; Wong et al., 2002a,
73 2002b), and oxygen mass balance (Bushinsky and Emerson, 2015; Emerson, 1987; Emerson et
74 al., 1991, 1993; Giesbrecht et al., 2012; Juranek et al., 2012; Plant et al., 2016).

75 **2 Methods**

76 **2.1 Measurements of O₂, DIC, and phytoplankton biomass**

77 Autonomous in situ oxygen measurements were made on a profiling float deployed by
78 the University of Washington (Special Oxygen Sensor Argo float, SOS-Argo F8397, WMO #



79 5903743, Figure 1). The complete dataset is available at
80 <https://sites.google.com/a/uw.edu/sosargo/>, and some of the data have been published previously
81 by Bushinsky and Emerson (2015) and Yang et al. (2017). Oxygen measurements on the SOS-
82 Argo float were obtained using an Aanderaa optode oxygen sensor with air-calibration
83 mechanism (Bushinsky et al., 2016) capable of providing the air-sea difference in oxygen
84 concentration with an accuracy of about $\pm 0.2\%$ and a vertical resolution of 3-5 m in the top 200
85 m of water column. This float was operated at a cycle interval of ~ 5 days covering depths from
86 surface to 1800 m.

87 Partial pressure of seawater CO_2 ($p\text{CO}_2$), temperature, and salinity data were obtained
88 from the NOAA mooring at OSP (WMO # 4800400). The complete dataset is available at
89 http://cdiac.ornl.gov/oceans/Moorings/Papa_145W_50N.html, and some of the data were
90 published by Fassbender et al. (2016). DIC was calculated using the total alkalinity (TA)- $p\text{CO}_2$
91 pair in CO2sys program Version 1.1 (van Heuven et al. 2011), where TA was calculated using
92 the linear relationship with salinity developed in Fassbender et al. (2016) ($\text{TA} = 37 \times S + 988$)
93 for the OSP vicinity. The calculation was performed on the total pH scale using the carbonate
94 dissociation constants (K_1' and K_2') of Lueker et al. (2000), the HSO_4^- dissociation constant from
95 Dickson et al. (1990), and the B_T/S ratio from Lee et al. (2010). The DIC data were normalized
96 to the annual mean salinity at OSP (32.5), to eliminate the influence from evaporation/dilution.

97 Water samples for phytoplankton abundance and community composition were collected
98 at OSP during 14 Line P repeat hydrographic cruises aboard the CCGS John P. Tully from 2012
99 to 2016 (February, June, and August for each year). Phytoplankton biomass, measured as total
100 chlorophyll *a* (chl-*a*) concentrations, and the contribution of the main taxonomic groups of
101 phytoplankton to chl-*a* were determined from high performance liquid chromatography (HPLC)



102 measurements of phytoplankton pigment concentrations (chlorophylls and carotenoids, Zapata
103 et al. 2000) followed by CHEMTAX v1.95 analysis (Mackey et al., 1996). Eight algal groups
104 were included in the chemotaxonomic analysis: diatoms, haptophytes, chlorophytes,
105 pelagophytes, prasinophytes, dinoflagellates, cryptophytes, and cyanobacteria. However,
106 cryptophytes were not found since their biomarker pigment, alloxanthin was not detected in any
107 of our samples. Pigment ratios for each algal group were obtained from Higgins et al. (2011) and
108 used as ‘seed’ values for multiple trials (60 runs) from randomized starting points, as described
109 by Wright et al. (2009). The same initial pigment ratios (Table 1a) were used in all cruises but
110 each cruise was run separately to allow potential variations in the CHEMTAX optimization to be
111 expressed. The range of final pigment ratios are given in Table 1b. The six best solutions (those
112 with the lowest residuals) were averaged for estimating the taxonomic abundances.

113 **2.2 Models used for NCP calculation**

114 **2.2.1 Oxygen mass balance model**

115 Oxygen, temperature, and salinity data from SOS-Argo F8397 and wind speed (U_{10}) data from
116 NOAA PMEL OSP mooring (<https://www.pmel.noaa.gov/ocs/data/disdell/>,
117 <https://www.pmel.noaa.gov/ocs/data/fluxdisdell/>) were used in a multi-layer upper ocean O_2
118 mass balance model to calculate NCP. This model frame (Figure 3) is similar to what was used
119 in Bushinsky and Emerson (2015), which compartmentalizes the upper ocean (0-150 m) into a
120 mixed layer box (with variable height) with one meter boxes below. This model assumes that
121 horizontal processes are not important. Because horizontal gradients of oxygen supersaturation
122 are small, lateral transport has much less influence on this property than fluxes from air-sea gas
123 exchange, vertical advection, and diapycnal eddy diffusion. A detailed assessment of this
124 assumption is given in Yang et al. (2017).



125 We define ANCP as the flux of organic carbon that escapes the “upper ocean” after a
126 complete seasonal cycle. To be consistent with this definition NCP is integrated vertically from
127 the surface ocean to the winter mixed layer depth, which in this location is roughly equal to the
128 pycnocline depth. Because internal waves cause a 10 to 20 meter variation in the depth of density
129 surfaces in this location, we used the annual mean pycnocline depth as the base of the modeled
130 “upper ocean” to conserve mass in the model. Fluxes across the base of the upper ocean are
131 calculated using measured gradients in oxygen at the density of the pycnocline, independent of
132 its depth.

133 Oxygen concentration changes over time in the modeled “upper ocean” with depth of h
134 ($dh[O_2]/dt$) are the sum of: gas exchange fluxes (F_{A-W}), vertical advection flux (F_V), diapycnal
135 eddy diffusion (F_{Kz}), entrainment between the mixed layer and the water below (F_E), and net
136 biological oxygen production (J_{NCP}).

$$\frac{dh[O_2]}{dt} = F_{A-W} + F_V + F_{Kz} + F_E + J_{NCP} \quad \text{mol m}^{-2} \text{ d}^{-1} \quad (1)$$

137

138 F_{A-W} is calculated only for the mixed layer box, using the a gas exchange model that includes
139 both diffusion and bubble processes (Emerson and Bushinsky, 2016; Liang et al., 2013). With
140 the time step (3 h) used in our case, the mixed layer change between time steps is always smaller
141 or equal to 1 m, so entrainment occurs only between the mixed layer box and the box below. The
142 entrainment flux (F_E) that gets out of the mixed layer box ends up going into the box below and
143 vice versa, so F_E for these two boxes have the same value but different signs and cancel each
144 other out. F_V is calculated from Ekman pumping rate (derived from wind speed) and oxygen
145 gradient from SOS-Argo measurements. F_{Kz} is calculated with oxygen gradient and diapycnal
146 eddy diffusion coefficient from Cronin et al. (2015), which decreases with depth from the base of



147 the mixed layer to a background value of $10^{-5} \text{ m}^{-2} \text{ s}^{-1}$ (Whalen et al., 2012) with a $1/e$ scaling
148 described in Sun et al. (2013) (See also Bushinsky and Emerson, 2015). For the mixed layer
149 reservoir F_{kz} and F_V are considered only at the base of the box. For all the boxes below the mixed
150 layer, F_{kz} and F_V are considered both on the top and at the base of each box. Biological oxygen
151 production, J_{NCP} , is the difference between the calculated fluxes and the measured time rate of
152 change (left hand side of Equation 1). This value is converted from oxygen to carbon production
153 (i.e. ANCP) using a constant oxygen to carbon ratio of 1.45 (Hedges et al., 2002).

154 The uncertainty of ANCP was estimated using a Monte Carlo approach. Confidence
155 intervals for oxygen measurements and the gas exchange mass transfer coefficients used in the
156 oxygen mass balance model were assigned to the model, and varied randomly while ANCP was
157 calculated in two hundred runs for each calculation. Details of this approach are presented in the
158 supporting information and Yang et al. (2017).

159 **2.2.2 DIC mass balance model**

160 We used a similar mass balance model for DIC, in which the base of the modeled “upper
161 ocean” is set to the annual mean pycnocline depth (the same as the oxygen mass balance model).
162 This choice of the upper ocean depth distinguishes this model from the mixed layer model used
163 in Fassbender et al. (2016). Fluxes at the base of the upper ocean in our model use DIC
164 gradients, diapycnal eddy diffusion coefficients, and upwelling velocities determined at the mean
165 pycnocline depth while Fassbender et al. (2016) used the values at the bottom of the mixed layer.
166 Because the OSP surface mooring provided only the mixed layer DIC data, we assumed that
167 there is no annual net DIC change in the depth region between the mixed layer and the annual
168 mean pycnocline depth. The depth gradient of DIC used to calculate fluxes across the
169 pycnocline was calculated from measured oxygen gradients assuming dO_2/dz to $dDIC/dz$ ratio of



170 1.45 (Hedges et al., 2002). Thus, we assume for this calculation that the DIC change at the
171 pycnocline depth is only due to degradation of organic matter, which ignores the change due to
172 CaCO₃ dissolution (Fassbender et al., 2016). For the DIC mass balance the multi-layer model is
173 equivalent to a one-layer model:

$$\frac{dh[\text{DIC}]}{dt} = F_{A-W} + F_V + F_{Kz} + F_E + J_{NCP} \quad \text{mol m}^{-2} \text{d}^{-1} \quad (2)$$

174

175 where the DIC change ($dh[\text{DIC}]/dt$) for the modeled upper ocean (the air–sea interface to the
176 mean depth of the pycnocline) is due to air-water CO₂ exchange (F_{A-W}) at the air-sea interface,
177 vertical advection (F_V) and diapycnal eddy diffusion (F_{Kz}) at the base of the modeled “upper
178 ocean”, and net biological carbon production (J_{NCP}) in between. For this one-layer model,
179 entrainment occurred within the same layer (box) and therefore there is no net entrainment flux
180 ($F_E = 0$). The air-sea gas-exchange mass transfer coefficient is calculated as a function of wind
181 speed using equations from Wanninkhof (2014). The DIC gradients used for F_V and F_{Kz} are
182 derived from oxygen gradients at the pycnocline depth as described above.

183 **2.3 Temperature dependence of NCP derived from the metabolic theory of ecology**

184 The correlation between NCP variation and environmental temperature could be
185 attributed to the temperature dependence of planktonic metabolism. Regaudie-De-Gioux and
186 Duarte (2012) derived the temperature dependences of gross primary production (GPP) and
187 community respiration (CR) using the metabolic theory of ecology and a large historical dataset
188 on volumetric planktonic metabolism in different seasons and ocean regimes (1156 estimates of
189 volumetric metabolic rates and the corresponding water temperature). Equations 3 & 4 below are
190 their linear regressions between the natural logarithm of the specific metabolic rates ($GPP/Chla$
191 and $CR/Chla$) and the inverted water temperature ($1/kT$),



$$\ln \frac{GPP}{Chla} = a_p \frac{1}{kT} + b_p \quad (3)$$

$$\ln \frac{CR}{Chla} = a_r \frac{1}{kT} + b_r \quad (4)$$

192

193 where *Chla* is the chlorophyll-*a* concentration, *k* is the Boltzmann's constant, *T* is the
 194 environmental temperature in Kelvin, and *a_p*, *b_p*, *a_r*, *b_r* are slopes and intercepts for each linear
 195 regression. The temperature dependence of *GPP/CR* can be derived by combining Equations
 196 3 & 4:

$$\frac{GPP}{CR} = EXP \left[(a_p - a_r) \frac{1}{kT} + (b_p - b_r) \right] \quad (5)$$

197

198 Since the community respiration (CR) includes the respiration of both autotrophs and
 199 heterotrophs, NCP can be calculated as the difference between GPP and CR.

$$NCP = GPP - CR = GPP \left(1 - \frac{CR}{GPP} \right) \quad (6)$$

200 Combining Equations 5 and 6 gives us the NCP-temperature relationship.

$$NCP = GPP \left\{ 1 - \frac{1}{EXP[(a_p - a_r) \frac{1}{kT} + (b_p - b_r)]} \right\} \quad (7)$$

201

202 3 Results

203 3.1 Oxygen and DIC measurements

204 The evolutions of density, oxygen concentration, and the oxygen anomaly in percent
 205 supersaturation ($\Delta O_2 = ([O_2]/[O_2]_{sat} - 1) \times 100$) determined by the profiling float at OSP from 2012
 206 to 2016 are presented in Figure 4(a-c). The saturation concentration of oxygen ($[O_2]_{sat}$) was
 207 calculated using equations from Garcia and Gordon (1992, 1993). The thin black line indicates



208 the mixed layer depth, which is defined by a density offset from the value at 10 m using a
209 threshold of 0.03 kg m^{-3} (de Boyer Montégut, 2004). The thick blue line indicates the pycnocline
210 with a density of $\sigma_{\theta} = 25.8 \text{ kg m}^{-3}$, which follows $[\text{O}_2]$ gradients well (Figure 4b). The white
211 boxes indicate the modeled “upper ocean” for each year, in which base of the modeled “upper
212 ocean” is the mean pycnocline depth for each year. Oxygen in the mixed layer was
213 supersaturated from mid April to October/November, and near saturation or slightly
214 undersaturated for the rest of the year (Figure 4c).

215 The evolution of salinity normalized DIC in the mixed layer determined by the OSP
216 mooring is presented in Figure 4d. The $p\text{CO}_2$ sensor stopped working during two periods in 2013
217 and 2016 (indicated with dash line boxes), and therefore the data for these two periods is filled
218 with interpolated values. Strong summertime DIC drawdown was observed in each year with the
219 lowest DIC around September.

220 **3.2 Annual Net Community Production**

221 All the terms of the oxygen mass balance calculation in each year are presented in Table
222 2a. The ANCP results (2.4 ± 0.6 , 0.8 ± 0.4 , 2.1 ± 0.4 and $1.6 \pm 0.4 \text{ mol C m}^{-2} \text{ yr}^{-1}$, with a mean
223 value of $1.7 \pm 0.7 \text{ mol C m}^{-2} \text{ yr}^{-1}$) indicate that ANCP initially decreased after warmer water
224 invaded this area (2013-14) and then returned to the “pre-blob” value of 2012-13 in subsequent
225 years. Given the uncertainty in the estimate of ANCP in each year, the value during year 2013-
226 14 is significantly different at the 95% confidence interval (as determined by t-test, Bethea et al.,
227 1975). With the exception of the unusually low value for 2013-14, ANCP values from oxygen
228 mass balance calculation are very close to the historical ANCP estimates at OSP ($2.3 \pm 0.6 \text{ mol}$
229 $\text{C m}^{-2} \text{ yr}^{-1}$, Emerson 2014).



230 If we integrate the ANCP from the ocean surface to the depth of the mixed layer
231 (ANCP_{mixed layer} in Table 2a) instead of to the annual mean depth of the pycnocline, the results are
232 higher (3.4, 1.3, 2.3 and 2.3 mol C m⁻² yr⁻¹, with a mean value of 2.4 ± 0.9 mol C m⁻² yr⁻¹).
233 While the mean value is higher because it includes some organic carbon flux that is degraded
234 between the mixed layer and pycnocline in summer, the annual trend, in which ANCP is
235 significantly lower in year two (2013-14), is the same as that in which ANCP values were
236 determined for the depth interval above the pycnocline.

237 In comparison, ANCP values determined from DIC mass balance are 2.0, 2.1, 2.6, 3.0
238 mol C m⁻² yr⁻¹, with a mean value of 2.4 ± 0.5 mol C m⁻² yr⁻¹ (Table 2b). The mean value is
239 similar within the errors of the value determined from the oxygen mass balance (1.7 ± 0.7 mol C
240 m⁻² yr⁻¹) but there is no significant change between the second year (2013-14) and those before
241 and after. The somewhat higher value could be due to the assumption we made about DIC
242 change below the mixed layer or because we neglected horizontal advection (See Discussion).

243 **3.3 Phytoplankton abundance and community composition**

244 Chl-*a* concentration, an indicator of phytoplankton biomass, was about 50% lower (0.22
245 mg m⁻³) during the period from August 2013 to June 2014 than during the rest of the 2012 to
246 2016 period (Figure 5a) and the historical annual average at OSP (Peña and Varela, 2007). Chl-*a*
247 resumed to the 2012-13 level in August 2014 and had a significant increase in the summer of
248 2016. 19'-hexanoyloxyfucoxanthin (Hex), which is mainly derived from prymnesiophytes, was
249 found to be the most abundant pigment after T-chla (Figure 5b). Fucoxanthin (Fuco), a pigment
250 associated with diatoms, haptophytes and pelagophytes, was also abundant and showed increased
251 concentration (0.54 mg m⁻³) in June 2016, coinciding with increased T-chla. After Hex, and
252 Fuco, chlorophyll-b was the most abundant pigment (0.36 to 0.27 mg m⁻³), indicating the



253 presence of green algae. We also detected occasionally lutein ($0-0.125 \text{ mg m}^{-3}$), violaxanthin ($0-$
254 0.012 mg m^{-3}) and, prasinoxanthin ($0-0.005 \text{ mg m}^{-3}$), which are biomarkers for green algae.

255 The CHEMTAX analysis detected the presence of seven classes of phytoplankton
256 (Figure 5c) and showed an increase in the relative contribution of cyanobacteria and
257 chlorophytes during the “Blob” period with the highest proportion of the former group in June of
258 2014 and the latter in June 2015 (Figure 5c). There was also a decrease in the abundance of
259 diatoms from August 2013 to June 2015. The remainder of the phytoplankton community was
260 primarily composed of haptophytes and the contribution of the other phytoplankton groups was
261 variable and showed no consistent year-to-year variability. By August 2015 the phytoplankton
262 community had returned to a similar relative composition as observed in 2012-13, with
263 nanoplankton (mostly haptophytes) being dominant and with microplankton (diatoms and
264 dinoflagellates) increasing in abundance. The input matrix (Table 1a) appeared to describe the
265 environment well since the final pigment ratio matrix did not differ dramatically from the initial
266 input values.

267 **4 Discussion**

268 **4.1 Comparisons of ANCP from oxygen and DIC mass balances**

269 Although the ANCP are integrated to the same depth in our oxygen and DIC mass
270 balance models, as mentioned in Section 3.2, the ANCP determined from DIC mass balance (4-
271 year mean: $2.4 \pm 0.5 \text{ mol C m}^{-2} \text{ yr}^{-1}$) is somewhat higher than the value determined from oxygen
272 mass balance (4-year mean: $1.7 \pm 0.7 \text{ mol C m}^{-2} \text{ yr}^{-1}$), but still within the error of the model.
273 There are two possible reasons for such discrepancy. First of all, due to the lack of DIC data
274 below the mixed layer, for the DIC model we made an assumption that there is no annual net
275 DIC change in the depth region between the mixed layer and the annual mean pycnocline depth.



276 With this assumption, the ANCP from DIC mass balance is higher because it includes the
277 organic carbon that is degraded between the mixed layer and pycnocline in summer, so the
278 ANCP from DIC mass balance (4-year mean: $2.4 \pm 0.5 \text{ mol C m}^{-2} \text{ yr}^{-1}$) is very similar to the
279 mixed layer ANCP determined from our oxygen mass balance model (4-year mean: 2.4 ± 0.9
280 $\text{mol C m}^{-2} \text{ yr}^{-1}$) and the mixed layer ANCP determined by Fassbender et al. (2016) ($2 \pm 1 \text{ mol C}$
281 $\text{m}^{-2} \text{ yr}^{-1}$). The second possible reason that the 4-year mean value of ANCP determined from the
282 DIC mass balance is higher than the value determined from the oxygen mass balance is
283 horizontal advection. Because gas exchange resets the oxygen saturation anomaly for oxygen
284 about ten times faster than CO_2 , the DIC mass balance is more vulnerable to horizontal fluxes
285 than the O_2 mass balance. If we assumed that the difference in ANCP estimated from these two
286 tracers ($0.7 \text{ mol C m}^{-2} \text{ yr}^{-1}$) is due to horizontal advection, and calculate the horizontal DIC
287 gradient using the 4-year mean horizontal velocity at OSP of 0.08 m s^{-1} , we found that a
288 horizontal DIC gradient of $1 \times 10^{-8} \text{ mol m}^{-4}$ is required to cause the difference of $0.7 \text{ mol C m}^{-2} \text{ yr}^{-1}$
289 ¹, which is possible at this location (horizontal DIC gradient along the 4-year mean horizontal
290 flow at OSP is about $2\sim 3 \times 10^{-8} \text{ mol m}^{-4}$ from GLODAP v1.1 gridded product, Key et al., 2004).

291 As for the inter-annual changes in ANCP, the oxygen mass balance calculation shows
292 that ANCP had a significant decrease in 2013-14 and then returned to the “pre-blob” level in the
293 following years whereas ANCP calculated from DIC mass balance does not show this trend.
294 Since air-sea exchange is a large part of the flux mass balance for both oxygen and CO_2 (Table
295 2), a likely reason for this discrepancy is due to the shorter residence time with respect to gas
296 exchange for the oxygen compared to the CO_2 saturation anomalies. An example of the residence
297 time calculation is included in the supporting information where it indicates that the gas
298 exchange residence time in the upper ocean for oxygen is about one month and that for CO_2 is



299 about one year (See also Emerson and Hedges, 2008, Chapter 11). Thus, the biologically induced
300 saturation anomaly for oxygen responds fast enough to record annual changes whereas that for
301 $p\text{CO}_2$ and DIC does not. On the other hand, as discussed above, since DIC mass balance is more
302 vulnerable to horizontal flux than oxygen mass balance, the DIC signal might already been
303 “smoothed” by the horizontal flux, which may also explain why the inter-annual ANCP changes
304 were not observed by using the DIC mass balance approach. The sharp decrease in ANCP from
305 the oxygen mass balance in 2013-14 is consistent with the decrease in chlorophyll concentration
306 by about 50% observed for the same period (Figure 5a). Hence, from this point forward we will
307 focus on analyzing the factors that might influence ANCP variations determined by the oxygen
308 mass balance model.

309 **4.2 Causes of ANCP decrease**

310 In the following paragraphs, we analyze connections between ANCP decrease and the
311 “Blob” temperature anomaly in the context of multiple physical and biological processes,
312 including the choices of start time from which ANCP are calculated, the base depth of the
313 modeled “upper ocean”, planktonic metabolism, and changes in phytoplankton community
314 composition.

315 Our observations began in June 2012, 10 – 12 months before the positive SST anomalies.
316 To determine whether the start date for determining the ANCP values affects the results, we
317 began the time series on four different months (Table 3). We are somewhat limited because
318 there is only about 12 “pre-blob” months before June, 2012. However, as shown in Table 3, as
319 long as there are more “pre-blob” months than “Blob-affected” months in the 1st year, the
320 significant ANCP decrease from 1st to 2nd year is still observed and the trend of ANCP variation
321 for those 4 years remains.



322 To determine whether the annual mean pycnocline depth (the white rectangles in Figure
323 4a-4c) influences the ANCP trends we calculated ANCP using the 4-year mean depth of 100 m
324 for the modeled “upper ocean”. The ANCP results only change slightly (2.6, 1.0, 1.9, and 1.6
325 mol C m⁻² yr⁻¹) and the decrease in 2013-14 is still statistically significant, indicating that the
326 different base depth used for the modeled “upper ocean” is not the key factor that causes ANCP
327 changes.

328 To test if the temperature dependence of planktonic metabolism is strong enough to
329 cause the ANCP decline we observed (e.g. 1.6 mol C m⁻² yr⁻¹ between 2012-13 and 2013-14), we
330 calculated the GPP from measured NCP of year 1 (2012-13) using Equation 7, and assumed GPP
331 was constant for all four years so we could then determine the effect of temperature on NCP
332 based on the metabolic theory of ecology (Equation 7). Since the specific phytoplankton growth
333 rate increases with increasing temperature (e.g. Regaudie-De-Gioux and Duarte, 2012; Chen and
334 Laws, 2017), if phytoplankton biomass would have remained the same during the “blob”, GPP
335 would have increased. Thus, assuming a constant GPP in this calculation is somewhat
336 speculative, but it at least provides a first order assessment of the metabolic temperature effect on
337 ANCP. The parameterizations derived with datasets from Arctic were used (Regaudie-De-Gioux
338 and Duarte, 2012), because it gives the largest change in ANCP. The results (Table 4) indicate
339 that temperature dependence of planktonic metabolism is not strong enough to account for the
340 measured ANCP decrease in the 2nd year (2013-14), suggesting that this is not the major reason
341 for the observed ANCP decline.

342 Having ruled out the above likely candidates, we suggest that the low phytoplankton
343 biomass observed in the 2nd year (2013-14, Figure 5a), and the observed change in phytoplankton
344 community composition (Figure 5c) are the most likely causes for the ANCP decrease. In



345 general, larger phytoplankton (i.e. microplankton) are more efficient exporters than smaller
346 nanoplankton and picoplankton (e.g., Chen and Laws, 2016). Given the lower export rates of
347 picoplankton (e.g. cyanobacteria) than those of larger phytoplankton (e.g. diatoms) the observed
348 changes in phytoplankton community composition (Figure 5b) in 2013-14, which included a
349 decrease in the relative abundance of diatoms, and an increase in the relative abundance of
350 cyanobacteria and green algae (chlorophytes), could have further contributed to the decrease in
351 ANCP. After the initial response to the temperature anomaly, chl-*a* concentration and the
352 phytoplankton community composition returned to a level similar to those observed before the
353 warming occurred, suggesting that the plankton community rapidly adapted to the higher
354 temperature.

355 **5 Conclusions**

356 The annual net community production (ANCP) at Ocean Station Papa (OSP) in the
357 subarctic Northeast Pacific Ocean was determined from June 2012 to June 2016 to examine the
358 effect of the temperature anomaly on the efficiency of carbon export. The ANCP determined by
359 oxygen mass balance had a four year mean value of $1.7 \pm 0.7 \text{ mol C m}^{-2} \text{ yr}^{-1}$, whereas ANCP
360 determined by DIC mass balance gives a somewhat higher mean value ($2.4 \pm 0.5 \text{ mol C m}^{-2} \text{ yr}^{-1}$).
361 ANCP for individual years determined from O₂ mass balance showed a significant decrease in
362 year 2 (2013-14) after the onset of the temperature anomaly, but no significant decrease in
363 ANCP was found when calculated with DIC mass balance. We believe that this indicates that
364 the DIC concentration and *p*CO₂ respond too slowly to capture annual changes in ANCP. Based
365 on our observations and historical ANCP estimates at OSP as reference, we found there was a
366 significant ANCP decrease in 2013-14 due to the warm anomaly, which is consistent with the
367 findings from concurrent phytoplankton data. Possible mechanisms for the observed decrease in



368 ANCP by the oxygen mass balance in the second year were analyzed in the context of multiple
369 physical and biological processes that could be affected by temperature anomaly. Our analysis
370 showed that the ANCP decrease was most likely due to changes in phytoplankton abundance and
371 community composition after the “Blob” entered the area.

372

373 ***Data availability.***

374 Float data are available online (<https://sites.google.com/a/uw.edu/sosargo/home>). Mooring data
375 is available online at: http://cdiac.ornl.gov/oceans/Moorings/Papa_145W_50N.html.

376 ***Author contributions.***

377 BY and SRE designed the experiments. BY developed the model code and process the data. AP
378 provided the phytoplankton data. BY and SRE prepared the manuscript with contributions from
379 all co-authors.

380 ***Competing interests.***

381 The authors declare that they have no conflict of interest.

382 ***Acknowledgements.***

383 We thank Dr. Stephen Riser and Dana Swift for their assistance in development of the SOS-Argo
384 float, and scientists of NOAA PMEL and the Institute of Ocean Sciences (IOS) and crews of
385 CCGS John P. Tully, for their work on OSP mooring and Line P cruises. Special thanks are
386 given to Dr. John Crusius for the constructive discussions and comments on this study. This
387 work was supported by National Science Foundation grant OCE-1458888.

388 **References**

389 Allen, A. P., Gillooly, J. F. and Brown, J. H.: Linking the global carbon cycle to individual
390 metabolism, *Funct. Ecol.*, 19(2), 202–213, doi:10.1111/j.1365-2435.2005.00952.x, 2005.
391 Bethea, R. M., Duran, B. S. and Boullion, T. L.: *Statistical methods for engineers and scientists*,
392 Marcel Dekker, Inc., New York., 1975.



- 393 Bond, N. A., Cronin, M. F., Freeland, H. and Mantua, N.: Causes and impacts of the 2014 warm
394 anomaly in the NE Pacific, *Geophys. Res. Lett.*, 42(9), 3414–3420, doi:10.1002/2015GL063306,
395 2015.
- 396 de Boyer Montégut, C.: Mixed layer depth over the global ocean: An examination of profile data
397 and a profile-based climatology, *J. Geophys. Res.*, 109(C12), C12003,
398 doi:10.1029/2004JC002378, 2004.
- 399 Brown, J. H., Gillooly, J. F., Allen, A. P., Savage, V. M. and West, G. B.: TOWARD A
400 METABOLIC THEORY OF ECOLOGY, *Ecology*, 85(7), 1771–1789, doi:10.1890/03-9000,
401 2004.
- 402 Bushinsky, S. M. and Emerson, S.: Marine biological production from in situ oxygen
403 measurements on a profiling float in the subarctic Pacific Ocean, *Global Biogeochem. Cycles*,
404 29(12), 2050–2060, 2015.
- 405 Bushinsky, S. M., Emerson, S. R., Riser, S. C. and Swift, D. D.: Accurate oxygen measurements
406 on modified Argo floats using in situ air calibrations, *Limnol. Oceanogr. Methods*, 2016.
- 407 Cavole, L., Demko, A., Diner, R., Giddings, A., Koester, I., Pagniello, C., Paulsen, M.-L.,
408 Ramirez-Valdez, A., Schwenck, S., Yen, N., Zill, M. and Franks, P.: Biological Impacts of the
409 2013–2015 Warm-Water Anomaly in the Northeast Pacific: Winners, Losers, and the Future,
410 *Oceanography*, 29(2), 273–285, doi:10.5670/oceanog.2016.32, 2016.
- 411 Charette, M. A., Bradley Moran, S. and Bishop, J. K. B.: as a tracer of particulate organic carbon
412 export in the subarctic northeast Pacific Ocean, *Deep Sea Res. Part II Top. Stud. Oceanogr.*,
413 46(11–12), 2833–2861, doi:10.1016/S0967-0645(99)00085-5, 1999.
- 414 Chen, B. and Laws, E. A.: Is there a difference of temperature sensitivity between marine
415 phytoplankton and heterotrophs?, *Limnol. Oceanogr.*, doi:10.1002/lno.10462, 2016.
- 416 Cronin, M. F., Pelland, N. A., Emerson, S. R. and Crawford, W. R.: Estimating diffusivity from
417 the mixed layer heat and salt balances in the North Pacific, *J. Geophys. Res. Ocean.*, 120(11),
418 7346–7362, 2015.
- 419 Dickson, A. G., Wesolowski, D. J., Palmer, D. A. and Mesmer, R. E.: Dissociation constant of
420 bisulfate ion in aqueous sodium chloride solutions to 250. degree. C, *J. Phys. Chem.*, 94(20),
421 7978–7985, 1990.
- 422 Emerson, S.: Seasonal oxygen cycles and biological new production in surface waters of the
423 subarctic Pacific Ocean, *J. Geophys. Res. Ocean.*, 92(C6), 6535–6544, 1987.
- 424 Emerson, S. and Bushinsky, S.: The role of bubbles during air-sea gas exchange, *J. Geophys.*
425 *Res. Ocean.*, 2016.
- 426 Emerson, S. and Hedges, J.: Chemical oceanography and the marine carbon cycle., 2008.
- 427 Emerson, S. and Stump, C.: Net biological oxygen production in the ocean—II: Remote in situ
428 measurements of O₂ and N₂ in subarctic pacific surface waters, *Deep Sea Res. Part I Oceanogr.*
429 *Res. Pap.*, 57(10), 1255–1265, 2010.
- 430 Emerson, S., Quay, P., Stump, C., Wilbur, D. and Knox, M.: O₂, Ar, N₂, and 222Rn in surface
431 waters of the subarctic Ocean: Net biological O₂ production, *Global Biogeochem. Cycles*, 5(1),
432 49–69, doi:10.1029/90GB02656, 1991.
- 433 Emerson, S., Quay, P. and Wheeler, P. A.: Biological productivity determined from oxygen mass
434 balance and incubation experiments, *Deep Sea Res. Part I Oceanogr. Res. Pap.*, 40(11), 2351–
435 2358, 1993.
- 436 Emerson, S., Sabine, C., Cronin, M. F., Feely, R., Cullison Gray, S. E. and DeGrandpre, M.:
437 Quantifying the flux of CaCO₃ and organic carbon from the surface ocean using in situ
438 measurements of O₂, N₂, pCO₂, and pH, *Global Biogeochem. Cycles*, 25(3), n/a-n/a,



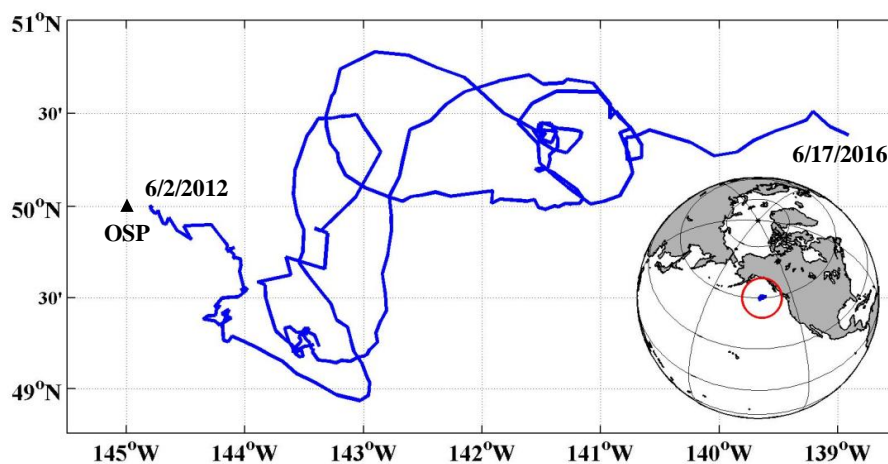
- 439 doi:10.1029/2010GB003924, 2011.
- 440 Fassbender, A. J., Sabine, C. L. and Cronin, M. F.: Net community production and calcification
441 from 7 years of NOAA Station Papa Mooring measurements, *Global Biogeochem. Cycles*, 30(2),
442 250–267, doi:10.1002/2015GB005205, 2016.
- 443 Freeland, H.: A short history of Ocean Station Papa and Line P, *Prog. Oceanogr.*, 75(2), 120–
444 125, doi:10.1016/j.pocean.2007.08.005, 2007.
- 445 Freeland, H. J. and Cummins, P. F.: Argo: A new tool for environmental monitoring and
446 assessment of the world’s oceans, an example from the N.E. Pacific, *Prog. Oceanogr.*, 64(1), 31–
447 44, doi:10.1016/j.pocean.2004.11.002, 2005.
- 448 Garcia, H. E. and Gordon, L. I.: Oxygen solubility in seawater: Better fitting equations, *Limnol.*
449 *Oceanogr.*, 37(6), 1307–1312, doi:10.4319/lo.1992.37.6.1307, 1992.
- 450 Garcia, H. E. and Gordon, L. I.: Erratum: Oxygen Solubility in Seawater: Better Fitting
451 Equations, *Limnol. Ocean.*, 38(3), 656 [online] Available from:
452 <http://www.jstor.org/stable/2838040?seq=1>, 1993.
- 453 Giesbrecht, K. E., Hamme, R. C. and Emerson, S. R.: Biological productivity along Line P in the
454 subarctic northeast Pacific: In situ versus incubation-based methods, *Global Biogeochem.*
455 *Cycles*, 26(3), doi:10.1029/2012GB004349, 2012.
- 456 Gillooly, J. F., Brown, J. H. and West, G. B.: Effects of Size and Temperature on Metabolic
457 Rate, *Science* (80-.), 293(September), 2248–2252, doi:10.1126/science.1061967, 2001.
- 458 Hedges, J. I., Baldock, J. A., G??linas, Y., Lee, C., Peterson, M. L. and Wakeham, S. G.: The
459 biochemical and elemental compositions of marine plankton: A NMR perspective, *Mar. Chem.*,
460 78(1), 47–63, doi:10.1016/S0304-4203(02)00009-9, 2002.
- 461 van Heuven, S., Pierrot, D., Rae, J. W. B., Lewis, E. and Wallace., D. W. R.: MATLAB Program
462 Developed for CO₂ System Calculations. ORNL/CDIAC-105b., ,
463 doi:10.3334/CDIAC/otg.CO2SYS_MATLAB_v1.1, 2011.
- 464 Higgins, H. W., S. W. Wright, and L. Schlüter. 2011. Quantitative interpretation of
465 chemotaxonomic pigment data, p. 257-313. In S. Roy, C. A. Llewellyn, E. S. Egeland, and G.
466 Johnsen [eds.], *Phytoplankton Pigments: Characterization, Chemotaxonomy, and Applications in*
467 *Oceanography*. Cambridge University Press.
- 468 Johnson, K. S., Berelson, W. M., Boss, E. S., Claustre, H., Emerson, S. R., Gruber, N.,
469 Körtzinger, A., Perry, M. J. and Riser, S. C.: Observing Biogeochemical Cycles at Global Scales
470 with Profiling Floats and Gliders: Prospects for a Global Array, *Oceanography*, 22 [online]
471 Available from: <http://dx.doi.org/10.5670/oceanog.2009.81>, 2009.
- 472 Juranek, L. W., Quay, P. D., Feely, R. A., Lockwood, D., Karl, D. M. and Church, M. J.:
473 Biological production in the NE Pacific and its influence on air-sea CO₂ flux: Evidence from
474 dissolved oxygen isotopes and O₂/Ar, *J. Geophys. Res. Ocean.*, 117(C5), n/a-n/a,
475 doi:10.1029/2011jc007450, 2012.
- 476 Key, R. M., Kozyr, A., Sabine, C. L., Lee, K., Wanninkhof, R., Bullister, J. L., Feely, R. A.,
477 Millero, F. J., Mordy, C. and Peng, T. H.: A global ocean carbon climatology: Results from
478 Global Data Analysis Project (GLODAP), *Global Biogeochem. Cycles*, 18(4), 1–23,
479 doi:10.1029/2004GB002247, 2004.
- 480 Lee, K., Kim, T.-W., Byrne, R. H., Millero, F. J., Feely, R. A. and Liu, Y.-M.: The universal
481 ratio of boron to chlorinity for the North Pacific and North Atlantic oceans, *Geochim.*
482 *Cosmochim. Acta*, 74(6), 1801–1811, 2010.
- 483 Liang, J. H., Deutsch, C., McWilliams, J. C., Baschek, B., Sullivan, P. P. and Chiba, D.:
484 Parameterizing bubble-mediated air-sea gas exchange and its effect on ocean ventilation, *Global*



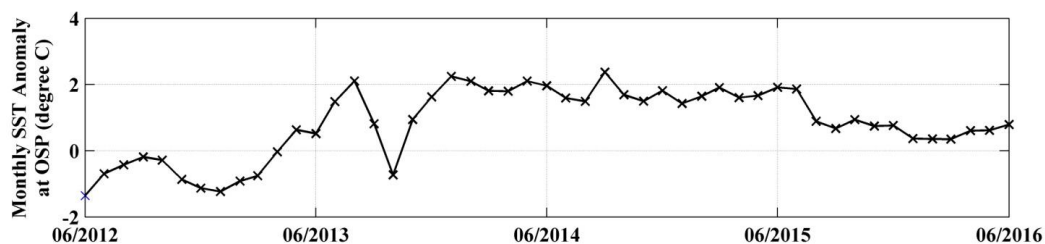
- 485 Biogeochem. Cycles, 27(3), 894–905, doi:10.1002/gbc.20080, 2013.
- 486 López-Urrutia, A., San Martín, E., Harris, R. P. and Irigoien, X.: Scaling the metabolic balance
487 of the oceans., Proc. Natl. Acad. Sci. U. S. A., 103(23), 8739–44, doi:10.1073/pnas.0601137103,
488 2006.
- 489 Di Lorenzo, E. and Mantua, N.: Multi-year persistence of the 2014/15 North Pacific marine
490 heatwave, Nat. Clim. Chang., (July), 1–7, doi:10.1038/nclimate3082, 2016.
- 491 Lueker, T. J., Dickson, A. G. and Keeling, C. D.: Ocean pCO₂ calculated from dissolved
492 inorganic carbon, alkalinity, and equations for K₁ and K₂: validation based on laboratory
493 measurements of CO₂ in gas and seawater at equilibrium, Mar. Chem., 70(1), 105–119, 2000.
- 494 Mackey, M. D., Mackey, D. J., Higgins, H. W. and Wright, S. W.: CHEMTAX - A program for
495 estimating class abundances from chemical markers: Application to HPLC measurements of
496 phytoplankton, Mar. Ecol. Prog. Ser., 144(1–3), 265–283, doi:10.3354/meps144265, 1996.
- 497 Peña, M. A. and Varela, D. E.: Seasonal and interannual variability in phytoplankton and nutrient
498 dynamics along Line P in the NE subarctic Pacific, Prog. Oceanogr., 75(2), 200–222,
499 doi:10.1016/j.pocean.2007.08.009, 2007.
- 500 Plant, J. N., Johnson, K. S., Sakamoto, C. M., Jannasch, H. W., Coletti, L. J., Riser, S. C. and
501 Swift, D. D.: Net community production at Ocean Station Papa observed with nitrate and oxygen
502 sensors on profiling floats, Global Biogeochem. Cycles, 30(6), 859–879,
503 doi:10.1002/2015GB005349, 2016.
- 504 Regaudie-De-Gioux, A. and Duarte, C. M.: Temperature dependence of planktonic metabolism
505 in the ocean, Global Biogeochem. Cycles, 26(1), doi:10.1029/2010GB003907, 2012.
- 506 Rose, J. M. and Caron, D. A.: Does low temperature constrain the growth rates of heterotrophic
507 protists? Evidence and implications for algal blooms in cold waters, Limnol. Oceanogr., 52(2),
508 886–895, doi:10.4319/lo.2007.52.2.0886, 2007.
- 509 Sun, O. M., Jayne, S. R., Polzin, K. L., Rahter, B. A. and St. Laurent, L. C.: Scaling Turbulent
510 Dissipation in the Transition Layer, J. Phys. Oceanogr., 43(11), 2475–2489, doi:10.1175/JPO-D-
511 13-057.1, 2013.
- 512 Takahashi, T., Olafsson, J., Goddard, J. G., Chipman, D. W. and Sutherland, S. C.: Seasonal
513 variation of CO₂ and nutrients in the high-latitude surface oceans: A comparative study, Global
514 Biogeochem. Cycles, 7(4), 843–878, doi:10.1029/93GB02263, 1993.
- 515 Wanninkhof, R.: Relationship between wind speed and gas exchange over the ocean revisited,
516 Limnol. Oceanogr. Methods, 12(JUN), 351–362, doi:10.4319/lom.2014.12.351, 2014.
- 517 Whalen, C. B., Talley, L. D. and MacKinnon, J. A.: Spatial and temporal variability of global
518 ocean mixing inferred from Argo profiles, Geophys. Res. Lett., 39(17),
519 doi:10.1029/2012GL053196, 2012.
- 520 Wong, C. ., Waser, N. A. ., Nojiri, Y., Whitney, F. ., Page, J. . and Zeng, J.: Seasonal cycles of
521 nutrients and dissolved inorganic carbon at high and mid latitudes in the North Pacific Ocean
522 during the Skaugran cruises: determination of new production and nutrient uptake ratios, Deep
523 Sea Res. Part II Top. Stud. Oceanogr., 49(24–25), 5317–5338, doi:10.1016/S0967-
524 0645(02)00193-5, 2002a.
- 525 Wong, C. S.: Analysis of trends in primary productivity and chlorophyll-a over two decades at
526 Ocean Station P (50°N, 145°W) in the subarctic northeast Pacific Ocean, Can. J. Fish. Aquat.
527 Sci., 121, 107–117 [online] Available from: <http://ci.nii.ac.jp/naid/10009665016/en/> (Accessed 4
528 February 2017), 1995.
- 529 Wong, C. S., Waser, N. A. D., Nojiri, Y., Johnson, W. K., Whitney, F. A., Page, J. S. C. and
530 Zeng, J.: Seasonal and Interannual Variability in the Distribution of Surface Nutrients and



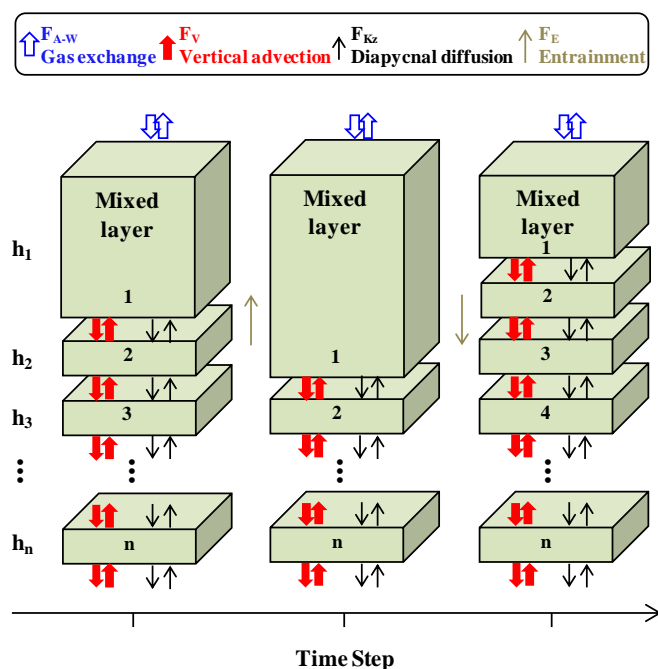
- 531 Dissolved Inorganic Carbon in the Northern North Pacific: Influence of El Niño, *J. Oceanogr.*,
532 | 58(2), 227–243, doi:10.1023/A:1015897323653, 2002b.
- 533 Wright, S. W., A. Ishikawa, H. J. Marchant, A. T. Davidson, R. L. VandenEnden, and G. V.
534 Nash. 2009. Composition and significance of picoplankton in Antarctic waters. *Polar Biol.* 32:
535 797–808.
- 536 Yang, B., Emerson, S. R. and Bushinsky, S. M.: Annual net community production in the
537 subtropical Pacific Ocean from in-situ oxygen measurements on profiling floats., *Global*
538 *Biogeochem. Cycles*, doi:10.1002/2016GB005545, 2017.
- 539 Zapata, M., F. Rodrigues, and J. L. Garrido. 2000. Separation of chlorophylls and carotenoids
540 from marine phytoplankton: a new HPLC method using a reversed phase C-8 column and
541 pyridine-containing mobile phases. *Mar. Ecol. Prog. Ser.* **195**: 29–45. doi:10.3354/meps195029.
542



543
544 **Figure 1** Study area and float path from 2012 to 2016. The black triangle indicates the position
545 of Ocean Station Papa (OSP) Mooring, and the blue line indicates the trajectory of the SOS-Argo
546 float which was within roughly a 2° (N-S) \times 6° (E-W) box.
547

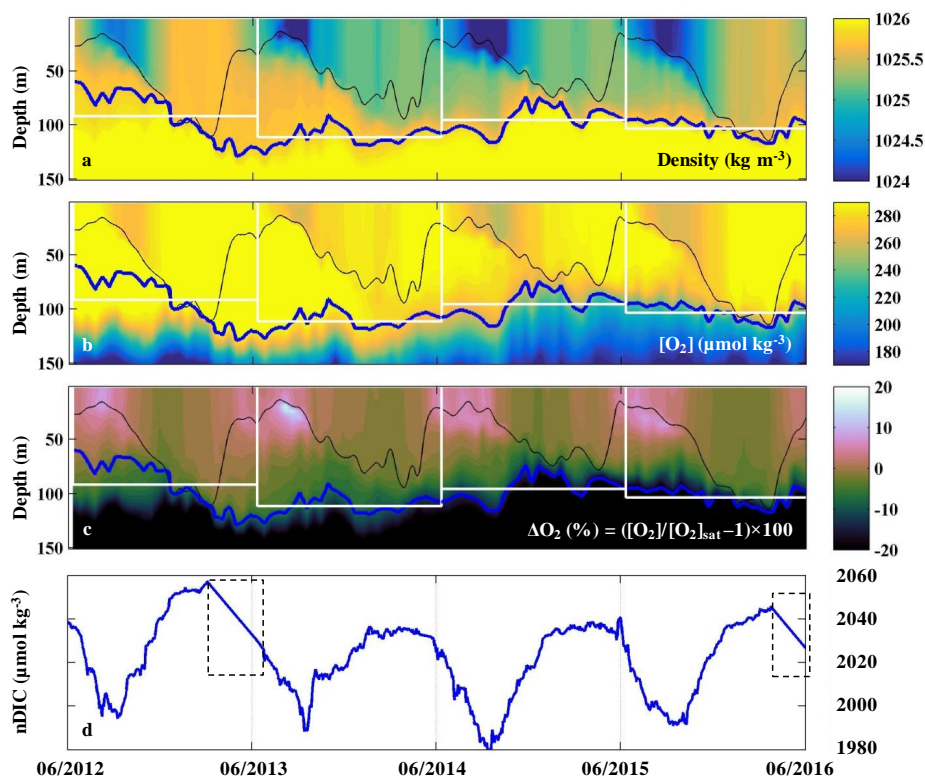


548
549 **Figure 2** Monthly SST Anomaly at Ocean Station Papa (OSP). The anomaly is defined as the
550 difference between the measured SST and the mean of 1971-2000. Data are from:
551 http://iridl.ldeo.columbia.edu/maproom/Global/Ocean_Temp/Anomaly.html
552

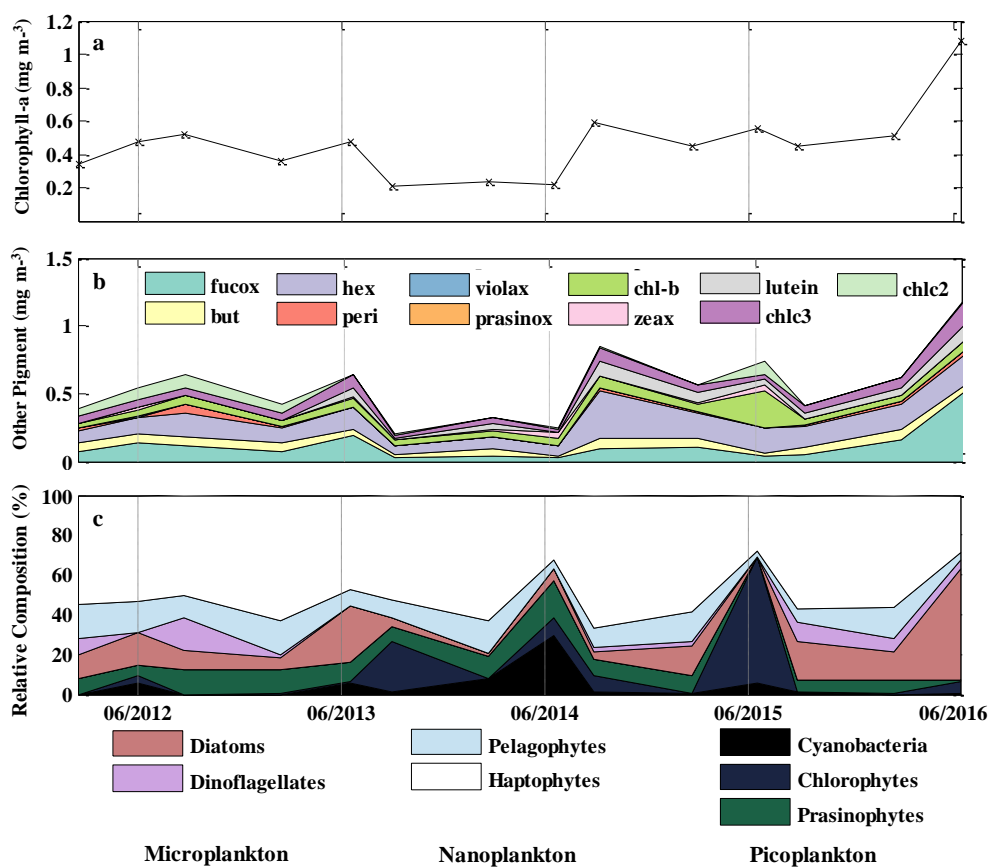


553
554
555
556
557
558

Figure 3 Schematic of the multi-layer upper ocean oxygen mass balance model (adapted from *Bushinsky and Emerson, 2015*). Fluxes (F) are from air-sea gas exchange (F_{A-w} , including diffusion and bubble processes), vertical advection (F_v), diapycnal eddy diffusion (F_{Kz}), and entrainment (F_E).



559
560 **Figure 4** (a-c) Upper ocean density, oxygen concentration, and oxygen supersaturation ΔO_2 (%)
561 from the SOS-Argo float at OSP. The thin black line indicates the mixed layer depth, the thick
562 blue line indicates the pycnocline depth, and the white rectangles indicate the modeled “upper
563 ocean” for each of the four years that ANCP were calculated. (d) Mixed layer DIC normalized to
564 a surface salinity at OSP ($S = 32.5$) from June 2012 to June 2016. Dash line boxes indicate
565 periods when the pCO_2 data were not available and thus were filled with a straight line
566 interpolation.



567

568

569

570

571

572

Figure 5 Mixed layer mean (a) chl-*a* concentration (mg m^{-3}), (b) other pigment concentration (mg m^{-3}), and (c) relative phytoplankton composition (%) at OSP. Values were determined from HPLC pigment analysis of samples collected in February, June, and August for each year from 2012 to 2016.



Table 1. Pigment:Chl *a* ratios for eight algal groups: (a) CHEMTAX initial ratio matrix, and (b) ranges of final pigment ratios obtained by CHEMTAX on the pigment data.

	Chl <i>c</i> ₃	Chl <i>c</i> ₂	Peri	But	Fuco	Pras	Viola	Hex	Allo	Zea	Lut	Chl <i>b</i>	Chl <i>a</i>
(a)													
Cyano	0	0	0	0	0	0	0	0	0	0.64	0	0	1
Chloro	0	0	0	0	0	0	0.049	0	0	0.032	0.17	0.32	1
Prasino	0	0	0	0	0	0.25	0.054	0	0	0.058	0.021	0.73	1
Crypto	0	0.2	0	0	0	0	0	0	0.38	0	0	0	1
Diatoms	0.08	0.28	0	0	0.99	0	0	0	0	0	0	0	1
Dinofla	0	0.22	0.56	0	0	0	0	0	0	0	0	0	1
Pelago	0.22	0	0	0.64	0.772	0	0	0	0	0	0	0	1
Hapto	0.18	0.21	0	0.039	0.289	0	0	0.47	0	0	0	0	1
(b)													
Cyano	0	0	0	0	0	0	0	0	0	0.48-0.85	0	0	1
Chloro	0	0	0	0	0	0	0.02-0.15	0	0	0.03-0.04	0.06-0.21	0.26-0.45	1
Prasin	0	0	0	0	0	0.04-0.23	0.02-0.06	0	0	0.02-0.06	0.017-0.022	0.72-1.12	1
Crypto	0	0.15-0.23	0	0	0	0	0	0	0.34-0.44	0	0	0	1
Diatoms	0.05-0.09	0.21-0.3	0	0	0.8-1.15	0	0	0	0	0	0	0	1
Dinofla	0	0.19-0.26	0.45-0.64	0	0	0	0	0	0	0	0	0	1
Pelago	0.11-0.25	0	0	0.68-1.15	0.22-0.82	0	0	0	0	0	0	0	1
Hapto	0.05-0.22	0.16-0.26	0	0.037-0.068	0.07-0.25	0	0	0.58-0.81	0	0	0	0	1

Abbreviations: Cyano, cyanobacteria; Chloro, chlorophytes; Prasino, prasinophytes; Crypto, cryptophytes; Dinofla, dinoflagellates; Pelago, pelagophytes; Hapto, haptophytes; Chl *c*₃, chlorophyll *c*₃; Chl *c*₂, chlorophyll *c*₂; Peri, peridinin; But, 19'-butanoyloxyfucoxanthin; Fuco, fucoxanthin; Pras, prasinoxanthin; Viola, violaxanthin; Hex, 19'-hexanoyloxyfucoxanthin; Allo, alloxanthin; Zea, zeaxanthin; Lut, lutein; Chl *b*, chlorophyll *b*; Chl *a*, chlorophyll.



Table 2 Annual net community production (ANCP) determined from (a) O₂ mass balance, and (b) DIC mass balance. The annually integrated fluxes for each of the important terms (columns 4-9) indicate that the air sea flux and biological production terms dominate for both tracers. Two ANCP values are given in (a): one integrated from the ocean surface to the depth of annual mean pycnocline (column 3), ANCP, and another value integrated over the depth of the mixed layer, ANCP_{mixed layer}. Only the former is a measure of the biological organic carbon that escapes the upper ocean on an annual basis (see text).

a										
Year	Time Period (June to June)	h (m)	Annual oxygen mass balance (mol O ₂ m ⁻² yr ⁻¹)						ANCP = J _{NCP} /1.45 (mol C m ⁻² yr ⁻¹)	ANCP _{mixed layer} (mol C m ⁻² yr ⁻¹)
			$dh[O_2]/dt = F_{A-W} + F_E + F_{Kz} + F_V + J_{NCP}$							
			$dh[O_2]/dt$	$F_{A-W} = F_s + F_b$	F_E	F_{Kz}	F_V	J_{NCP}		
1	2012-13	91	-0.7	-2.9	0	-0.6	-0.6	3.5	2.4 ± 0.6	3.4
2	2013-14	111	-1.3	-1.5	0	-0.8	-0.2	1.2	0.8 ± 0.4	1.3
3	2014-15	95	-0.6	-1.7	0	-0.9	-1.0	3.0	2.1 ± 0.4	2.3
4	2015-16	103	0.8	-0.1	0	-0.7	-0.3	2.3	1.6 ± 0.4	2.3
b										
Year	Time Period (June to June)	h (m)	Annual DIC mass balance (mol C m ⁻² yr ⁻¹)						ANCP = - J _{NCP} (mol C m ⁻² yr ⁻¹)	
			$dh[DIC]/dt = F_{A-W} + F_E + F_{Kz} + F_V + J_{NCP}$							
			$dh[DIC]/dt$	F_{A-W}	F_E	F_{Kz}	F_V	J_{NCP}		
1	2012-13	91	-0.2	1.0	0	0.7	0.1	-2.0	2.0	
2	2013-14	111	-0.1	1.5	0	0.4	0.1	-2.1	2.1	
3	2014-15	95	0.05	2.0	0	0.5	0.1	-2.6	2.6	
4	2015-16	103	-0.04	2.0	0	0.9	0.1	-3.0	3.0	



Table 3 ANCP calculated from O₂ mass balance with different start dates to determine if the chosen annual period affects the conclusions (see text).

	Start Time	6/10/12	7/10/12	8/10/12
	1 st year (2012-13)	2.4	2.3	2.4
ANCP	2 nd year (2013-14)	0.8	0.9	0.7
(mol C m ⁻² yr ⁻¹)	3 rd year (2014-15)	2.1	2.6	2.5
	4 th year (2015-16)	1.6	-	-



Table 4 Comparisons of ANCP measured with O₂ mass balance and ANCP predicted from the temperature dependence parameterization of planktonic metabolism using parameters from the Arctic Ocean [Regaudie-De-Gioux and Duarte, 2012]. Gross primary production (GPP) is calculated from ANCP in year 1 and Equation 7, and it is assumed to be the same through years 1 – 4. $ANCP_{diff} = 2.4 \text{ (mol C m}^{-2} \text{ yr}^{-1}) - ANCP_{Predicted \text{ or Measured}}$

Year	Mean temperature (°C)	ANCP (mol C m ⁻² yr ⁻¹)		ANCP _{diff} (mol C m ⁻² yr ⁻¹)	
		Predicted	Measured	Predicted	Measured
1	8.4	-	2.4	-	-
2	10.4	1.9	0.8	-0.5	-1.6
3	10.8	1.9	2.1	-0.5	-0.3
4	9.9	2.1	1.6	-0.3	-0.8